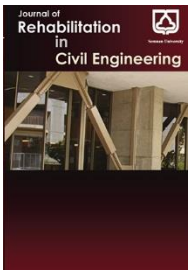

Journal homepage: http://civiljournal.semnan.ac.ir/

Geocell Reinforced Slope Behavior under Seismic Loading Using Calibrated Hypoplastic Soil Constitutive Model

Alireza Ardakani[1], Ali Namaei[1]

1. Department of Civil Engineering, Imam Khomeini International University, Qazvin, Iran
Corresponding author: namaeiali@edu.ikiu.ac.ir

ARTICLE INFO

Article history:
Received: 22 September 2020
Revised: 08 December 2020
Accepted: 01 May 2021

Keywords:
Hypoplastic;
Geocell;
Slope stability;
Inter granular strain.

ABSTRACT

This study evaluates geocell reinforced slope behavior under seismic loading using calibrated hypoplastic soil constitutive model. The constitutive soil model used in this simulation was calibrated for poorly graded dense sand by conducting a series of triaxial and odometer tests. A three dimensional analysis is carried out to simulate geocells and this soil model using the finite element software PLAXIS3D. To investigate the geocell seismic behavior, the lateral displacement, induced tensile force in geocell, slope stability and frequency content effect have been assessed. Furthermore, a comparison has been made among hypoplastic, Hardening soil with small strain and Mohr-Coulomb model. The obtained results indicated that the volumetric plastic strain and inter granular strain consideration by hypoplastic model had a significant effect on the lateral displacement of the reinforced and unreinforced slope. Using the geocell layers leaded to decrease the plastic points. This behavior caused to decrease the estimated results difference when performing three constitutive models as soil failure criterion. Also, the tensile force showed hypoplastic model was not sensitive to the earthquake reversible force. In addition, it was found that the geocells lost their effect when the PGA increased and the slope was apt to fail.

1. Introduction

Since past four decades high tensile resistance and polymeric materials have been industrialized. Soil reinforcement is one of the usages of these materials. Soil reinforcement is a popular way for stabilizing landslide, embankment, slopes, foundations and retaining walls because of their economic consideration, better performance under seismic loads, and ease of construction which it offers in comparison with conventional stabilization systems. Geocell layers are one type of three dimensional and

How to cite this article:
Ardakani, A., Namaei, A. (2021). Geocell Reinforced Slope Behavior under Seismic Loading Using Calibrated Hypoplastic Soil Constitutive Model. Journal of Rehabilitation in Civil Engineering, 9(4), 77-92.
https://doi.org/10.22075/JRCE.2021.21425.1446

honeycomb soil reinforcements which manufactured from polyethylene sheets using ultrasonically welded joints. This method confines the infilled soil by: (a) lateral resistance effect; (b) vertical stress dispersion effect; and (c) membrane effect, which make geocells proper for soil stabilization (Dash et al. 2003, Latha et al. 2008, Zhao et al. 2009, Latha and Manju 2016).

Firstly, Bathurst and Crowe (1992) evaluated the performance of geocells for stabilizing retaining walls and slopes. Latha and Rajagopal (2007) simulated an equivalent two dimensional numerical model to assess the effect of geocell in embankments reinforcing. They illustrated that the geocell was well-preserved as an equivalent soil layer with apparent cohesive strength and stiffness due to the geocell stabilization mechanism. Chen and Chiu (2008) physically modeled a geocell reinforced retaining wall. They indicated that the maximum lateral displacement decreases and occurred at the mid-height of the wall by placing geocell upper under static loading. Instead, the maximum lateral displacement increased by placing the geocell layers in the lower part of the wall. Ling et al. (2009) evaluated the geocell reinforced slope behavior under seismic loadings. They suggested the equivalent pseudo static coefficients for geocell retaining walls earthquake resistance examination. Mehdipour et al. (2013) evaluated the behavior of equivalent two dimensional geocell reinforced slope under static loads. The Mohr-Coulomb failure model was used to simulate the behavior of soil. They showed the optimum depth of the geocell placement and the effect of slope geometry, soil compaction and soil shear strength on the geocell behavior. Chen et al. (2013) assessed the behavior of the geocell reinforced retaining wall by using Mohr-Coulomb model. They indicated that a wall with a facing angle less than 80% will meaningfully decrease the lateral deflection of the wall face. Moreover, Mehidpour et al. (2017) compared the limit equilibrium safety factor of geocell reinforced slope with strength reduction method with Mohr-Coulomb criterion. They concluded that the limit equilibrium method is more conservative method to evaluate the geocell reinforced slope factor of safety. Song et al. (2018) investigated the failure geocell reinforced retaining wall mechanisms. Their results illustrated that failure surface was found to occur in geocell reinforced retaining walls when the apparent cohesion is very large, or the friction between the wall and the footing was small or there existed a weak interlayer in the wall similar to the failure mode of rigid retaining walls. Dai et al. (2018) used a series of physical tests to investigate the performance of embankment geocell reinforced under static and cyclic loading. They found that by placing the geocell layer shallower would cause higher slope stability of the embankment. Arvin et al. (2019) and Kazemian and Arvin (2019) used three dimensional strength reduction analyses to assess the behavior of geocell reinforced slope safety factor. They showed that the geocell layer forms a stiff layer which increases the slope safety factor by inducing a more uniform stress distribution. Song et al. (2019) recommended a new three dimensional numerical approach to simulate geocell reinforced foundation soils that the geocell was modeled as membrane elements and the complex interaction between geocell and soil was recognized by coupling their degrees of freedom. Their results indicated that the decrease in geocell pocket size has a significant effect on the bearing capacity increase. Also, it was found that the geocell thickness showed an insignificant influence

on the bearing capacity when the pocket size kept constant. Moreover, comparison with field data illustrated that this simulation method could efficiently predicted the behavior of geocell.

In the aforementioned investigations, numerical and experimental behavior of geocell reinforcement in slopes and retaining walls stabilization has been discussed. The numerical studies have employed simple soil constitutive models to simulate the behavior of geocell reinforced slopes or retaining walls. Still, no comprehensive studies are available to incorporate an advanced soil constitutive model for geocell reinforcement retaining walls and slopes. Therefore, more research is desired for developing reliable design and test methods for geocell usages in slope stability. Mohammadi Haji and Ardakani (2018) illustrated the influence of a soil constitutive model on prediction of seismic behavior of geotechnical engineer such as tunnel is irrefutable in numerical simulations.

Hypoplasticity is a particular class of incrementally nonlinear constitutive models, developed specially to predict the behavior of soils. The hypoplasticity model has been effectively used in numerical modeling of the response of sandy soil under cyclic loading (Bilotta et al. 2014, Lanzano et al. 2014, Mohammadi Haji and Ardakani, 2018). Hypoplasticity theory was first conducted by Wu and Kolymbas (1990), Wu and Bauer (1994), Kolymbas et al. (1995), Gudehus (1996) and Bauer (1996). In Hypoplasticity, there is no yield surface and this model is a comprehensive rate dependent model considered inter granular strain and it separates elastic and plastic strain increments. Moreover, hypoplastic model predicts other significant soil behavior such as critical state, the effect of soil density on shear strength, the effect of unloading and reloading on soil stiffness and monotonic and cyclic response of soil for small to large strains (Wu and Bauer 1994, Kolymbas et al. 1995, Bauer, 1996, Von Wolffersdorff 1996, Wu and Kolymbas 2000).

In this study, a comparison has been conducted between Mohr- Coulomb (MC), Hardening soil with small strain stiffness (HSS) and Hypoplastic model (H) in order to investigate seismic responses of a geocell reinforced slope. With the intention of evaluating this behavior, the slope factor of safety, induced forces and slope displacement have been measured. Furthermore, three different seismic loads were assessed in order to examine the effect of frequency contents on geocell reinforcement under seismic loading.

2. Numerical analysis and calibration

In this study, the behavior of geocell reinforced slope under seismic loading is investigated by using the finite element method. PLAXIS 3D finite element software was used to simulate the actual shape of geocell layers. The soil used for analysis was a dense Firooz kooh no. 161 which is poorly graded sand. As the soil constitutive model plays a key role to examine geocell seismic performance, the hypoplastic model for sand considered inter granular strain is obtained to simulate non-linear soil behavior incrementally. The tensorial equation for this constitutive model which is considered the effect of soil density and the effect of stress level is written as Eq (1). (Gudehus 1996).

$$\dot{T} = f_s L : D + f_s f_d N ||D|| \quad (1)$$

In this equation, $\dot{T}$ is the objective stress rate, D is the stretching rate and constitutive tensors and L and N are the fourth and second order of constitutive tensors,

respectively. Also, f_d and f_s are scalar factors considering the effect of the stress level and soil density, respectively (Gudehus, 1996). The hypoplastic model has fourteen parameters. These constitutive model parameters have been calibrated for Firooz kooh no. 161 by conducting a series of numerical analysis, triaxial and odometer tests (Mohammadi Haji and Ardakani 2020). The numerical evaluation is used to simulate the conducted tests with different input different hypoplastic parameters. The input parameters which have the best agreement with the experimental tests results, is selected as Firooz kooh no. 161 hypoplastic parameters. These parameters consist of φ_c critical state friction angle, e_{d0} the void ratio at maximum density, e_{i0} the maximum void ratio and e_{c0} the void ratio at critical state. Also, h_s and n are granulate hardness and exponent, respectively. The granulate hardness and its exponent are used to predict the compression line shape (Masin 2019). These parameters are calculated according to Eqs. (2) and (3) and the obtained Firooz kooh no. 161 compression line which is conducted from oedometer test according to ASTM D2435 and shown in Fig.1. Furthermore, e_{c0} is calculated through Eq. (4). In these equations p is mean effective stress, C_c is the tangent compression and e is void ratio at two different points of compression curve. Also, according to Masin (2019) suggestion the maximum void ratio e_{i0} and the void ratio at maximum density e_{d0} are calculated with Eqs. (5) and (6).

$$n = \frac{\ln(\frac{e_1 C_{c2}}{e_2 C_{c1}})}{\ln(\frac{p2}{p1})} \quad (2)$$

$$h_s = 3p(\frac{ne}{C_c})^{1/n} \quad (3)$$

$$e = e_{c0}\exp[-(\frac{3p}{h_s})^n] \quad (4)$$

$$e_{i0} = 1.2e_{c0} \quad (5)$$

$$e_{d0} = 0.5e_{c0} \quad (6)$$

In order to verify the oedometer test, a numerical modeling is conducted. An axisymmetric model was carried out by simulating a half of odometer test. Each loading step was applied to the specimen in different phases like testing condition. Parameters α and β appeared to be ineffective for the void ratio of the oedometer results and it was necessary to rely on their physical characteristics. Parameter α controls the peak friction angle, whereas β controls the bulk and shear stiffness. Thus, they should have no effect on the oedometer test results. Also, the void ratios (e_{c0}, e_{i0}, e_{d0}) was set according to aforementioned calculations (Mohammadi Haji and Ardakani 2020).

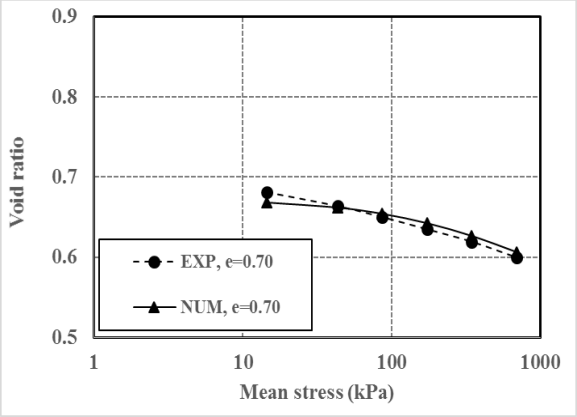

Fig. 1. The obtained compression curve for Firooz kooh no. 161 from oedometer test according to ASTM D2435 (Mohammadi Haji and Ardakani 2020).

Moreover, α and β are the basic parameters of granular hypoplastic model which control the peak friction angle and considering the density, respectively. Masin (2019) suggested that calculating these two parameters from a series of numerical sensitivity analyses and compare the obtained results from different values of α and β with a static drained triaxial test. Fig. 2 illustrates the results of monotonic drained triaxial tests compared to numerical simulations with different α and β which was evaluated by Mohammadi Haji and Ardakani

(2020). The consolidated drained triaxial test was conducted according to ASTM D7181 and an axisymmetric two dimensional model of this test was simulated, so the height of the specimen was set 75 cm like original test and the wide of specimen was set 18.75 cm to reach axisymmetric condition. The axisymmetric boundary was fixed to move and 100 kPa confining pressure was applied to the outer boundary of two dimensional specimen. Then four beta values (0.1, 0.5, 1 and 2) and five alpha values (0.1, 0.3, 0.4, 0.5, and 0.7) were used in plaxis hypoplastic soil constitutive model. It was observed that among the different numerical values for α and β, when $\alpha = 0.5$ and $\beta = 1$ the numerical results showed the best agreement with drained triaxial results.

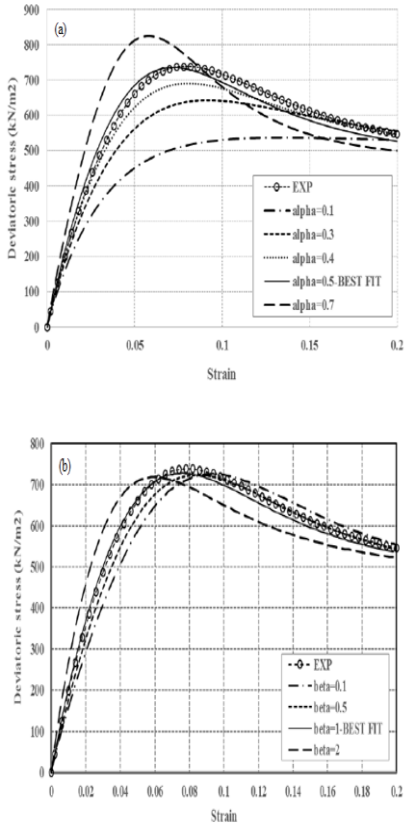

Fig. 2 Calibration Firooz kooh sand using measured and predicted static drained triaxial test according to ASTM D7181: a) *a* parameter, b) β parameter (Mohammadi Haji and Ardakani 2020).

On the other hand, m_R, m_T, R, β_r, χ are inter granular strain variables. m_R controls the initial shear modulus which is calculated from Eqs. (7-10). In these equations K is lateral earth coefficient at rest (Mohammadi Haji and Ardakani 2020).

$$G_0 = m_R \frac{h_s}{n}\left(\frac{3p_s}{h_s}\right)^{1-n}\left(\frac{e_{c0}}{e}\right)^{\beta} f_a f_k \quad (7)$$

$$f_k = 0.5\frac{(1+2K^2)+a^2(1-K)}{1+2K^2} \quad (8)$$

$$f_a = \left(\frac{e_{io}}{e_{co}}\right)^{\beta}\frac{1+e_{io}}{e_{io}}\left[3 + a^2 - a\sqrt{3}\left(\frac{e_{io}-e_{do}}{e_{co}-e_{do}}\right)^{\alpha}\right]^{-1} \quad (9)$$

$$a = \frac{\sqrt{3}(3-sin\phi_c)}{2\sqrt{2}\,sin\phi_c} \quad (10)$$

Parameter *R* relates to the elastic strain range, m_T represents the ratio of G_{90} to G_0, β_r controls the inter granular strain tensor, and χ controls the connection between the reversible and irreversible non-linear hypoplastic responses. These parameters cannot measure directly and a series of sensitivity analyses is needed. In order to calculate these parameters a drained consolidated cyclic triaxial test was conducted under 100 kPa confining pressure according to ASTM D5311. Same as the last part a numerical model was simulated with different values of m_T, R, β_r, χ. Eventually, Fig. 3 shows single hysteretic loop from drained cyclic triaxial test under 300 kPa confining pressure. From this figure the measured values are $m_R = 5$, $m_T = 2$, R = 1e-4, $\beta_r = 0.5$ and $\chi = 3$. Evaluation on this figure indicated that all numerical analysis have good compatibility with experimental tests. In addition to the aforementioned parameters, p_t is the parameter that shifts the mean stress due to the cohesion. In order to measure these parameters, a series of cyclic triaxial tests have been conducted for different parameters values. The final Firooz kooh no. 161 sand properties and hypoplastic

parameters which were obtained by Mohammadi Haji and Ardakani (2020) are listed in Table 1 and Table 2, respectively.

Moreover, the Mohr-Coulomb and Hardening soil with small strain parameters of this sand has been evaluated which is given in Table 3. The cohesion and friction angle of this sand have been calculated from direct shear test. Also, the secant modulus at 50% strength of triaxial test is denoted as E for Mohr-Coulomb. This value is considered as E_{50}^{ref} for HSS model. On the other hand, in order to calculate E_{ur}^{ref} and E_{oed}^{ref}, PLAXIS suggestion was used which recemmend to consider E_{ur}^{ref} and E_{oed}^{ref} as Eqs. (11) and (12), respectively.

$$E_{50}^{ref} = 1.25\, E_{oed}^{ref} \quad (11)$$

$$E_{ur}^{ref} = 3\, E_{50}^{ref} \quad (12)$$

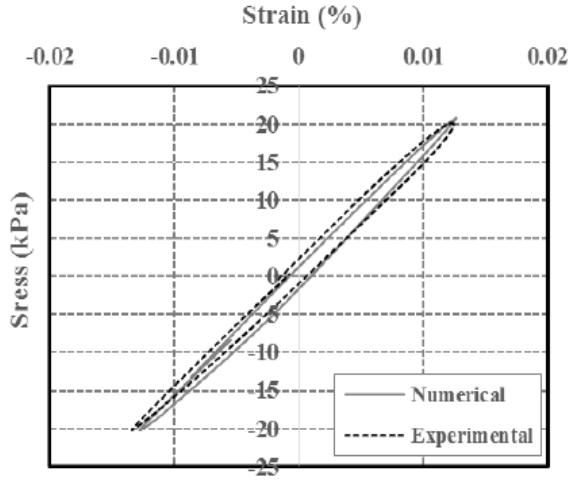

Fig. 3. Single hysteretic loop pressure using $m_T = 2$, R = 1e-4, $\beta_r = 0.5$ and $\chi = 3$ (Mohammadi Haji and Ardakani 2020).

Table 1. General properties of Firooz kooh sand (Mohammadi Haji and Ardakani 2020).

Properties	G_s	e_{max}	e_{min}	D_{50} (mm)	D_{10} (mm)	Unit weight (kN/m^3)
Sand	2.6	0.91	0.58	0.26	0.15	18

Table 2. Hypolastic parameters of Firooz kooh sand (Mohammadi Haji and Ardakani 2020).

Hypoplastic parameter	value
φ_c	32.7
n	0.24
h_s(kPa)	35e4
e_{c0}	0.91
e_{d0}	0.58
e_{i0}	1.1
α	0.5
β	1
m_R	5
m_T	2
R	1e-4
β_r	0.5
χ	3
p_t (kPa)	1

Table 3. Mohr-Coulomb and HSS parameters of Firooz kooh sand.

Model parameter	Value
Mohr-Coulomb	
C (kPa)	0.01
φ (Degree)	32.7
E (kPa)	14.8e3
HSS	
E_{50}^{ref} (kPa)	14.8e3
E_{oed}^{ref}(kPa)	11.85e3
E_{ur}^{ref} (kPa)	44.4e3
p^{ref}(kPa)	100
R_f	0.9

A 5 m height slope with 45 degree angle is used to investigate the seismic stability of geocell reinforced slope. Also, a geocell layer with 8 m length is modeled placed at 2 m from top of the slope in order to stabilize the

slope. Moreover, another geocell layer is placed at 4 m from the slope crest to assess the number of geocell layer effect.

A schematic view of the slope and equivalent diamond geocell simulated in this evaluation is illustrated in Fig. 1 in which S is the vertical geocell layers spacing, t and D indicate the geocell height and the distance to the side boundaries of the modeled zone, respectively.

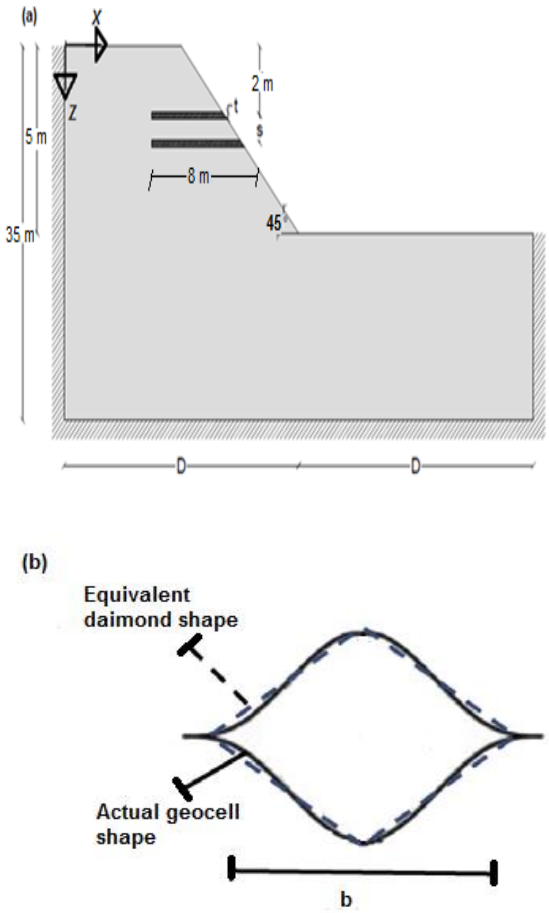

Fig. 4. A schematic view of the model used in this evaluation: a) Slope, b) Geocell.

In this study, the geocell layer is modeled as an equivalent diamond using geogrid elements in PLAXIS. Geogrid elements behave as an isotropic, linearly elastic material with no failure limit. Geogrid structural elements are flat elements that resist membrane but do not resist bending loading. The membrane stresses which develop in the geogrid balanced the effective confining stress and total shear stress. The interaction of geogrid with surrounding soil is calculated at each element node by a rigid attachment in the normal direction and a friction cohesion behavior in the tangent plane to the geogrid element surface. In this assessment, the geocell-soil interface coefficient is set as 2/3 in order to consider the effect of side interaction occurred between geocell pockets and filled martials as a result of vertical loading. This value is chosen, as a common value suggested by Leshchinsky and Ling (2013). The height, Young's modulus and aperture area of geogrid elements are set 100 mm, 160 kN/m and 25 cm × 25 cm, respectively. The input parameters of geocell are given in Table. 4. With the intention of evaluating the mesh dimensions a series of sensitivity analysis was conducted. The results indicated that the mesh size lower than medium size have no more influence on the analysis results. So, the medium mesh size has been chosen. Also, it has to be checked under each seismic loads that the mesh size do not be higher than 1/8 to 1/10 of wave length. Also, boundaries placed in 20 m from the slope crest along x- and y- direction. The sensitive analysis on the boundary distance from the bottom of model showed that the bedrock to be in 35 m from top of the slope. The final numerical model is illustrated in Fig. 5. Moreover, a part of three dimensional simulated geocell layer is shown in Fig. 6.

Table 4. Geocell parameters

Geocell properties	
Tensile yield strength (kN/m)	160
Height (mm)	100
Aperture size (cm × cm)	25 × 25

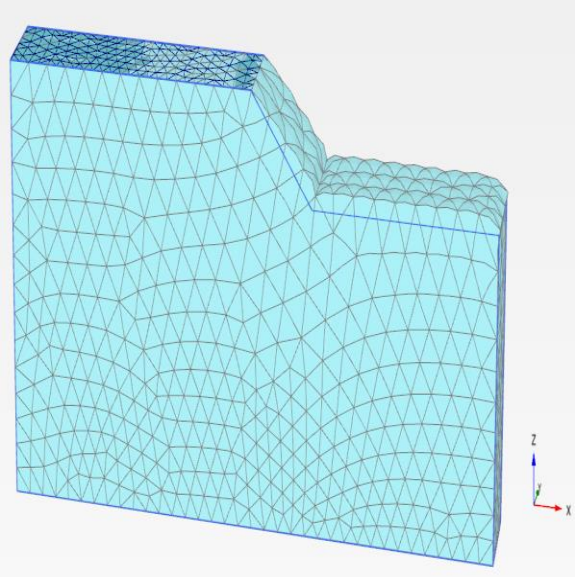

Fig. 5. Final numerical model.

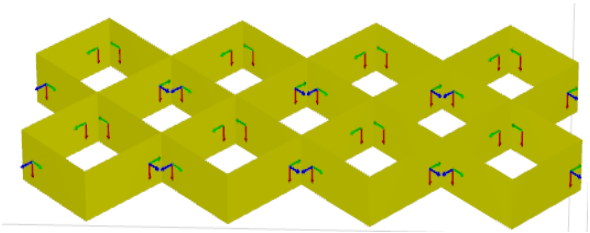

Fig. 6. A part of three dimensional simulated geocell.

In fully dynamic analysis, the time histories of El Centro 1940, Manjil 1990 and Trinidad 1983 earthquakes were applied as ground motion at 0.1 g, 0.2 g, 0.3 g and 0.6 g. The accelerations were selected to contain high ((PGA/PGV) > 1.2), medium (0.8 ≤ (PGA/PGV) ≤ 1.2) and low (0.8 < (PGA/PGV)) frequency contents (Kianoush and Ghaemmaghami, 2011). The time histories are applied at the bottom of the model along x-direction. The boundaries along x-direction and model bottom boundary were assumed to be viscous in order to prevent reflection. Also, the boundaries along y-direction and top of the model were set free. Table 5 shows the input motion properties and Fig. 7 depicts their time histories.

Table 5. Maximum acceleration and velocity of earthquake.

Earthquake record	Station	PGV (m/s)	PGA (g)	PGA/PGV
El Centro 1940	Imperial Valley	0.29	0.31	1.06
Manjil 1990	Abhar	0.55	0.21	0.38
Trinidad 1983	090 CDMG station 1498	0.08	0.19	2.37

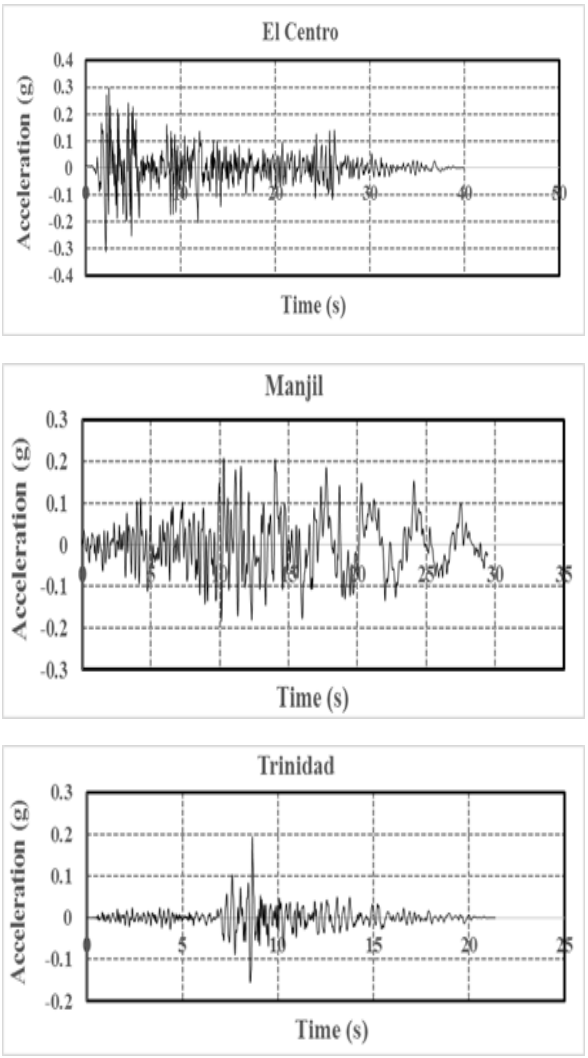

Fig. 7. Seismic load time histories.

3. Verification

The verification of the numerical analysis is validated by comparing the results with one model tests available report. Krishnaswamy et al. (2000) conducted a series of model tests on geocell reinforced slope. The slope was placed on a layer of geocell which used to reinforce the soft clay subgrade with 10 degree friction angle, 17 kN/m^3 unite weight, and 200 kPa Young's modulus.

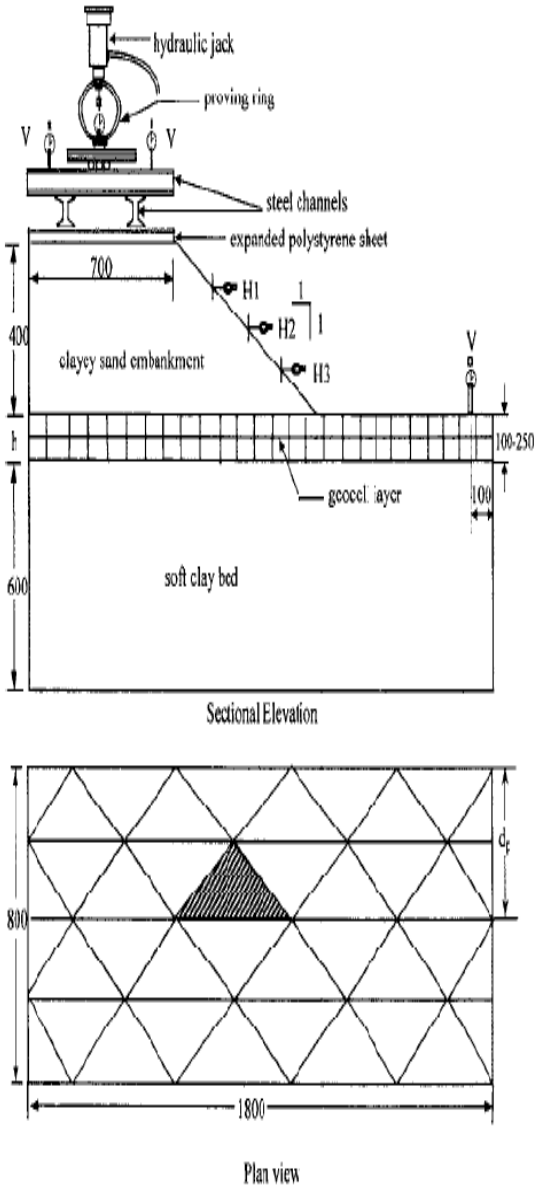

Fig. 8. The slope constructed by Krishnaswamy et al. (2000) for H1 (Unit: mm).

Above the geocell layer, the slope was constructed using clayey sand with 19 kN/m^3 Unite weight, 30 degree friction angle, and 10 kPa cohesion. The constructed slope chosen for verification is illustrated in Fig. 8. Mohr- Coulomb model were used to simulate soil failure yield criteria. Moreover, the surcharge was modeled by applying an equal displacement on the crest of the slope. The final finite element model of this embankment is illustrated in Fig. 9.

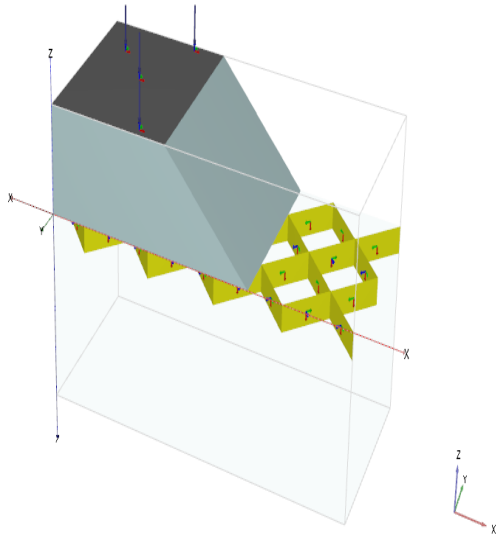

Fig. 9. Final finite element model of Krishnaswamy et al. (2000) embankment.

The numerical model was assessed in three phases. First, the initial stresses of soft clay are calculated in zero phase then the geocell layer is placed over the bed soil and the embankment constructed. Finally in the last phase, the surcharge is applied on the clayey sand embankment.

Fig. 10 illustrates the comparison between the 3D analysis and the experimental model test results for H1 LVDT presented by Krishnaswamy et al. (2000). It is observed that the lateral displacement and settlement in the numerical analysis conducted have good agreement with model tests that indicates the verification of the geocell reinforced slope behavior.

4. Results and discussion

In this section the seismic responses of a geocell reinforced slope is evaluated. In order to investigate this seismic behavior, the slope displacement, induced forces, frequency content and slope stability a series of numerical analyses have been conducted with three different soil models (Hypoplastic, Hardening Soil with Small strain and Mohr-Coulomb). The safety factor of geocell reinforced slopes is defined with a non-dimensional value called improvement factor calculated as Eq. (13). Wherein $SF_{reinforced}$ and $SF_{unreinforced}$ are the safety factor of reinforced and unreinforced slopes, respectively.

$$IF = \frac{SF_{reinforced}}{SF_{unreinforced}} \quad (13)$$

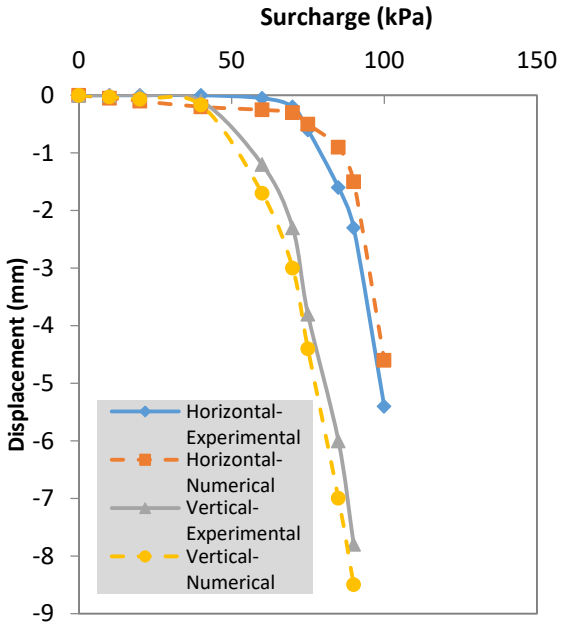

Fig. 10. Comparison between the obtained results and model tests of Krishnaswamy et al. for H1 (2000).

4.1. Comparison of different soil models

Figs. 11 and 12 illustrate the maximum lateral displacement response of the one geocell layer reinforced and unreinforced slope to El Centro 1940 with three soil constitutive models at 0.1 g, respectively. In these figures, the displacement is measure at 1 m from top of the slope and it is obvious that the obtained displacements from MC model are higher HSS than hypoplastic models in both the reinforced and unreinforced cases. This could be due to the Mohr-Coulomb inability to consider unloading and reloading behavior of soil accurately. As a result, the lateral displacement estimated by Mohr-Coulomb is nearly 50 % higher than hypoplastic model for reinforced case. This difference is more sensible for unreinforced case that the lateral displacement is predicted triple of hypoplastic displacement at the end of the earthquake. Also, by comparing between unreinforced and reinforced cases, it can present that the geocell mattresses decrease the slope volumetric plastic strain. Hence, the difference between Mohr-Coulomb and hypoplastic model is decreased due to the geocell mattress reduction effect on the volumetric plastic strain. Furthermore, the obtained results with HSS have a good agreement with the hypoplastic one generally. Although there is nearly 30 % lower at the end of the loading for both cases which indicates inter granular strain prediction with hypoplastic constitutive soil model. From the obtained results, it can be concluded that hypoplastic constitutive model can simulate the seismic reinforced and unreinforced slope behavior accurately while conventional model like Mohr-Coulomb gives conservative results.

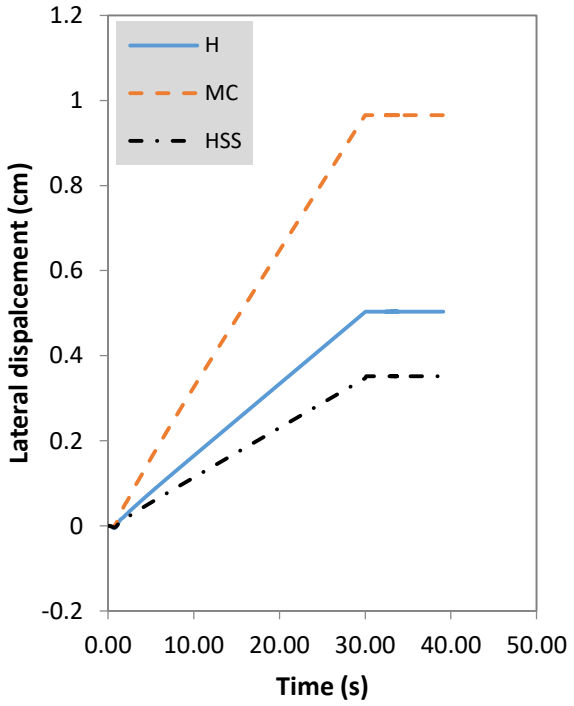

Fig. 11. Geocell reinforced slope the maximum lateral displacement time histories.

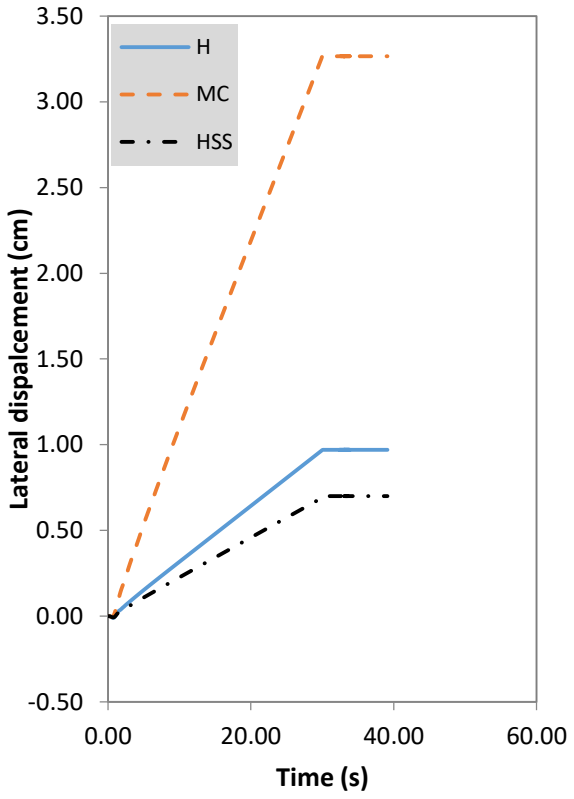

Fig. 12. Unreinforced slope lateral displacement time histories.

In addition to the displacement, the geocell tensile force has been demonstrated in Fig. 13. In these graphs, HSS and MC models estimate the tensile induced force in the geocells higher than hypoplastic model during earthquake. In HSS and MC, the maximum tensile force during earthquake is 10.5 and 17 kN/m while hypoplastic model predicts 7.5 kN/m at most. Also, it can be seen that the reversal force is lower in hypoplastic model while HSS and MC results show more sensitivity due to the earthquake reversible force. It may be related to MC and HSS models basis that cannot consider the hysteresis damping of soil and do not estimate the soil hysteresis loop. Hence, this lack of ability leads to capture higher tensile force during ground motion.

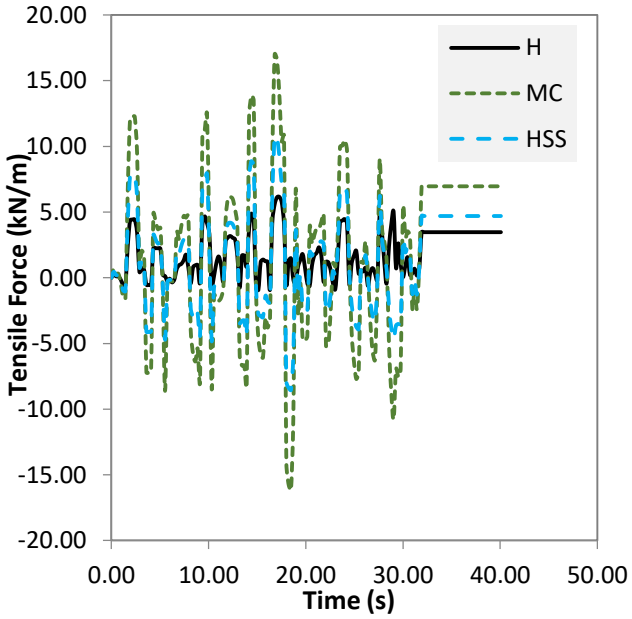

Fig. 13. Geocell tensile force time histories.

4.2. Slope stability

Table 6 gives unreinforced safety factor and IF factor for one and two geocell layers reinforcement with three different used soil constitutive models. As it was expected, two geocell layers give higher IF values than one layer. Then again, this Table demonstrates that the Mohr-Coulomb model has the lowest

unreinforced safety factor. These values validate the effect of simulating volumetric plastic strain that has not been considered by MC model. So, this model gives a conservative estimation for slope improvement and stability. Also, it can be seen that improvement factor values of hypoplastic model has the facility to calculate inter granular strain leaded to lower improvement factor than HSS model. Conversely, the obtained IF values indicate that all three models consider the improvement effect of geocell mattresses on the slope stability. This improvement can be assessed accurately when the number of geocell layers increased. This result shows that a geocell layer decreases the plastic strain and increase the slope stability. As the number of geocell layer increases, this reduction effect is increases too. This behavior causes to predict the slope stability improvement without any significant difference among all three constitutive models when two geocell layers are used. Moreover, it can be seen that the differences between safety factors for three models are lower than differences between lateral displacements and tensile forces. It can be stated that as these three models have a significant difference in strain calculation and do not considerably change soil strength parameters such as cohesion and friction, the effect of changing soil models for estimating slope safety factor is lower than displacement estimation.

Table 6. The obtained slope improvement and safety factor.

Constitutive model	MC	H	HSS
Unreinforced	1.06	1.17	1.20
One layer IF	1.13	1.18	1.21
Two layers IF	1.21	1.22	1.24

4.3. Frequency content

Fig. 14 shows the variation of slope maximum lateral displacement versus PGA for unreinforced, one layer and two layers geocell reinforced. An evaluation on these graphs indicates that the decrease in PGA leads to increase the slope maximum lateral displacement for both reinforced and unreinforced conditions. The maximum lateral displacement occurs under El Centro 1940 earthquake caused 1.8 cm displacement at 0.6 g for unreinforced slope. This value decreases to 1.5 cm and 1.3 cm as a result of placing the first and second geocell layers, respectively. It seems that the natural frequency of slope is closer to El Centro 1940 earthquake with medium frequency content ($0.8 \leq (PGA/PGV) \leq 1.2$ and PGA = 0.31) which causes a higher slope displacement at the same ground acceleration. In order to evaluate the efficiency of reinforcement on the lateral displacement, the displacement reduction value is calculated (DR) as Eq. (14).Where, A_U and A_R are the displacement amplitude of unreinforced and reinforced slope, respectively. Furthermore, it can be seen that the unreinforced maximum lateral displacement are higher than the reinforced cases by decreasing the PGA value. This may be due to the slope failure tendency by increasing the PGA and the lateral displacement increases.

$$DR = \frac{A_U - A_R}{A_U} \times 100 \quad (14)$$

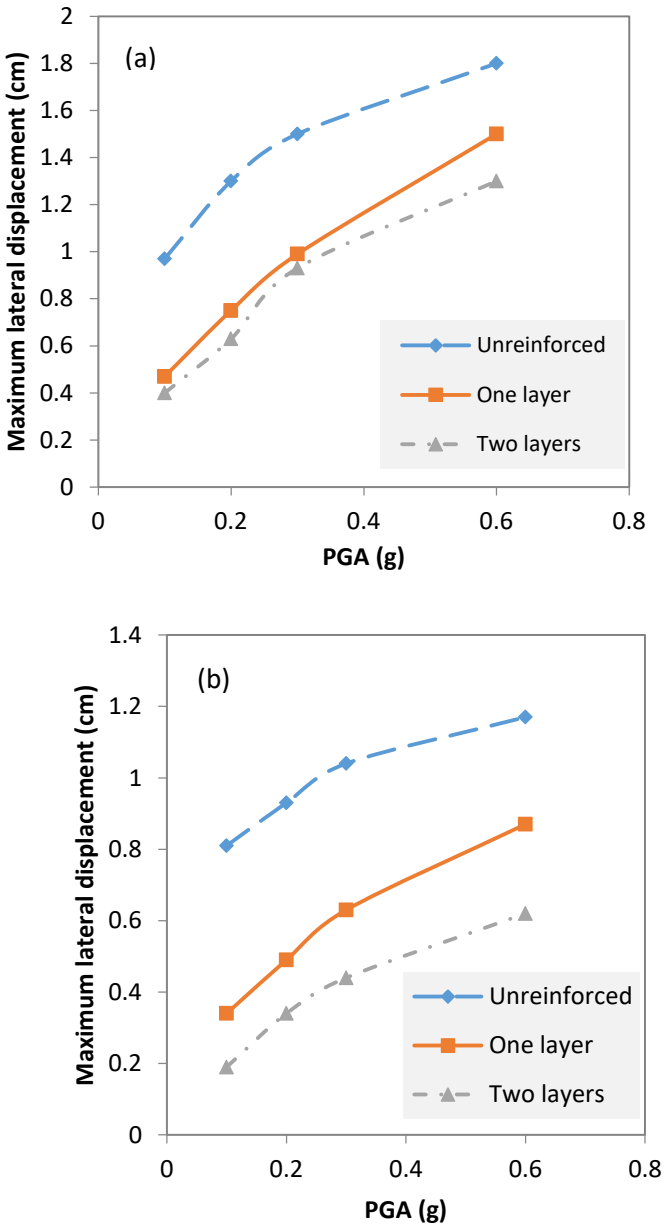

Fig. 14. Variation of maximum lateral displacement versus PGA: (a) El Centro, (b) Trinidad and (c) Manjil.

The calculated values of DR are illustrated in Fig. 15. This figure shows that the geocell reinforcement has a significant effect on the improvement of the slope seismic stability. One and Two geocell layers reduce the maximum lateral displacement 58 % and 76 % for Trinidad 1983 at 0.1 g, when the PGA is lower than 0.3 g, respectively. On the other hand, at the PGA higher than 0.3 g, the DR value for one and two layers are 18 % and 23 % for El Centro 1940 at 0.6 g, respectively. The obtained displacement reduction value indicates that the geocell mattresses lose their efficiency when the slope tends to fail under seismic loading. This efficiency reduction depends on the seismic loading frequency content and peak ground acceleration.

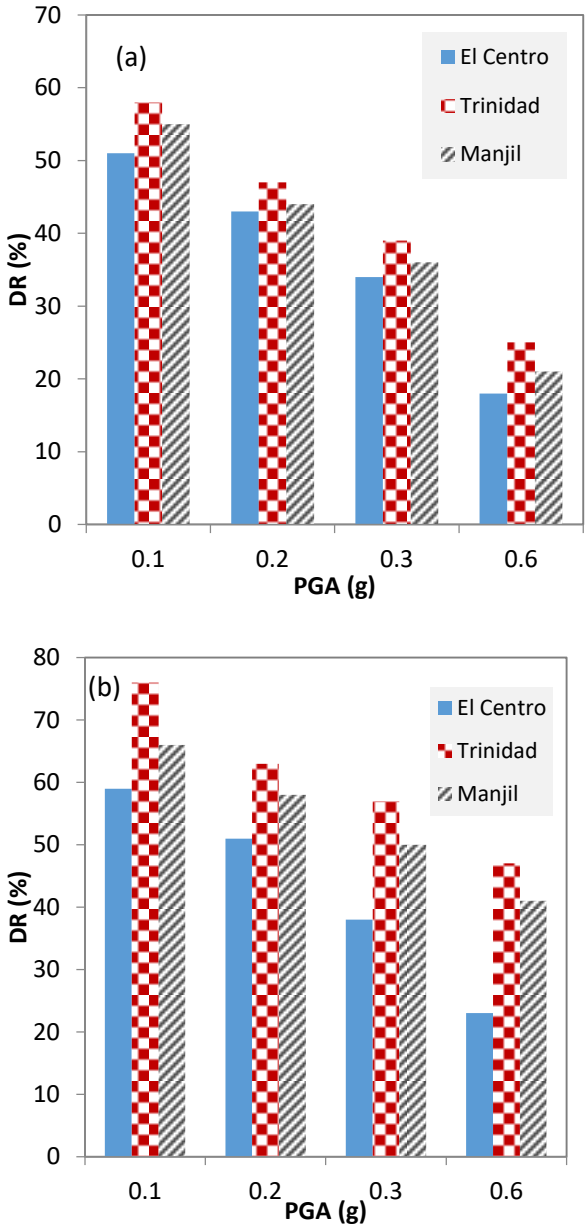

Fig. 15. Displacement reduction versus PGA: (a) Two layers and (b) One layer.

5. Conclusion

In the present research, a series of numerical modeling was conducted to assess the behavior of geocell reinforced slope under seismic loading using hypoplastic constitutive soil model. In these analyses the slope displacement, induced forces and slope stability have been investigated with Mohr-Coulomb, Hardening Soil with Small strain and hypoplastic constitutive soil models. Furthermore, the influence of seismic loading frequency content was evaluated by applying El Centro 1940, Manjil 1990 and Trinidad 1983 earthquakes as ground motion at 0.1 g, 0.2 g, 0.3 g and 0.6 g scale. Hence, the subsequent conclusions were drawn:

Based on the comparison among three different soil constitutive models for unreinforced and one layer geocell reinforced slope, the nonlinear hypoplastic model with considering inter granular strain had the ability to simulate the lateral slope displacement more realistically than Mohr-Coulomb and a nonlinear soil model like Hardening Soil with Small strain. These differences decreased in geocell reinforced slope point to the geocell mattresses reduction influence on the slope volumetric plastic strain. Furthermore, by comparing the three models induced geocell tensile forces demonstrated that the earthquake reversible force did not have significant effect on hypoplastic model induced geocell tensile force while HSS and MC results showed higher reversible tensile force.

Also, the slope stability evaluation verified the simulating volumetric plastic strain effect with hypoplastic model. It was found that the Mohr-Coulomb model predicted a conservative unreinforced slope safety factor. On the other hand, evaluating the slope stability improvement factor revealed that the geocell mattresses decreased the plastic strain. This effect was more sensible when the number of geocell layers increased. Increasing the geocell layers number leaded to decrease the plastic points. Therefore, there was not any significant difference among all three used soil constitutive models.

The results showed that the decrease in PGA leads to increase the slope maximum lateral displacement for both reinforced and unreinforced conditions. This behavior

showed that the modeled slope had a medium natural frequency ($0.8 \leq (PGA/PGV) \leq 1.2$) which was closer to El Centro 1940 earthquake frequency content with higher PGA than Manjil 1990 and Trinidad 1983 at the same ground acceleration. Additionally, it was found that the geocell layers are unable to apply their positive influence when the slope has a tendency to fail under different seismic loading.

Even though it was stated that hypoplastic model is needed a series of calibration tests but the obtained results encourage practicing designers to use this model for estimating more realistic results especially for seismic behavior estimation of reinforced slope. Also, it was observed that designers have to consider all frequency contents which can significantly affect the results. Still the current research only considered one geocell thickness, one geocell modulus, cell configuration and slope geometries, the results may not apply to other situations. Therefore, more comprehensive investigations are necessary to generalize standards for practical problems.

References

[1] Arvin, M. R., Zakeri, A., and Shoorijeh, M. B. (2019). "Using finite element strength reduction method for stability analysis of geocell-reinforced slopes." Geotechnical and Geological Engineering, 37(3), 1453-1467.

[2] ASTM D5311 (2013) Standard test methods for load controlled cyclic triaxial strength of soil, United States.

[3] ASTM D2435 (2004) Standard test methods for one-dimensional consolidation properties of soils, United States.

[4] ASTM D7181

[5] Bathurst R.J., and Crow, R.E. (1992). "Recent case histories of flexible geocell retaining walls in North America." In: Tatsuoka F, Leschinsky, D. (eds). Proceedings of conference on recent case histories of permanent geosynthetic reinforced soil retaining walls, Tokoyo, 3-20.

[6] Bauer, E. (1996). "Calibration of comprehensive hypoplastic model for granular materials." Soils and Foundation, 36, 13-26.

[7] Bilotta, E., Lanzano, G., Madabhushi, S.P.G., and Silvestri, F. (2014). "A nuemerical round robin on tunnels under seismic actions." Acta Geotechnica, 9(4), 563-579.

[8] Chen, R.H., and Chiu, Y.M. (2008). "Model tests of geocell retaining structures." Geotext. and Geomembr. 26, 56-70.

[9] Chen, R.H., Huang, Y.W., and Huang, F.C. (2013). "Confinement effect of geocells on sand samples under triaxial compression.' Geotext. and Geomembr. 37, 35-44.

[10] Dai, Z., Zhang, M., Yang, L., and Zhu, H., (2018). "Model tests on performance of embankment reinforced with geocell under static and cyclic loading." Proceedings of GeoShanghai International Conference: Ground Improvement and Geosynthetics, 399-410.

[11] Dash, S.K., Sireesh, S., and Sitharam, T.G., (2003). "Model studies on circular footing supported on geocell reinforced sand underlain by soft clay." Geotextiles and Geomembranes 21 (4), 197-219.

[12] Gudehus, G. (1994). "A Comprehensive Constitutive Equation for Granular Materials." Soils and Foundation 36(1), 1–12.

[13] Kazemian, T., and Arvin, M. R. (2019). "Three-dimensional stability of locally loaded geocell-reinforced slopes by strength reduction method." Geomechanics and Geoengineering, 14(3), 185-201.

[14] Kianoush, M.R., and Ghaemmaghami, A.R. (2011). "The effect of earthquake frequency content on the seismic behavior of concrete rectangular liquid tanks using the finite element method incorporating soil-structure interaction." Eng. Struct. 33, 186-200.

[15] Kolymbas, D., Herle, I., and Von Wolffersdorff, P.A. (1994). "Hypoplastic constitutive equation with internal

variables." Int. J. Numer. Anal. Met. 19, 415-36.

[16] Krishnaswamy, N.R., Rajagopal, K., and Latha, G., (2000). "Model studies on geocell supported embankments constructed over a soft clay foundation." Geotechnical Testing Journal, ASTM 23, 45-54.

[17] Lanzano, G., Bilotta, E., Russo, G., and Silvestri, F. (2014). "Experimental and Numerical Study on Circular Tunnels under Seismic Loading." European Journal of Environmental and Civil Engineering 19 (5), 539– 563.

[18] Latha, G.M., and Rajagopal, K., (2007). "Parametric finite element analyses of geocell supported embankments." Canadian Geotechnical Journal, 44 (8), 917-927.

[19] Latha, G.M., Dash, S.K., and Rajagopal, K., (2008). "Equivalent continuum simulations of geocell reinforced sand beds supporting strip footings." Geotechnical and Geological Engineering, 26, 387-398.

[20] Latha, G.M., and Manju, G.S. (2018). "Seismic response of geocell retaining walls through shaking table tests." Int. J. of Geosynth. and Ground Eng. 2(7), 1-15.

[21] Leshchinsky, B., and Ling, H.I., (2013a). "Effects of geocell confinement on strength and deformation behavior of gravel.' Journal of Geotechnical and Geoenvironmental Engineering 139 (2), 340-352.

[22] Ling, H.I., Leshchinsky, D., Wang, J.P., Mohri, Y., and Rosen, A., (2009). "Seismic response of geocell retaining walls: experimental studies". Journal of Geotechnical and Geoenvironmental Engineering, ASCE 135(4), 515-524.

[23] Masin, D. (2019). "Modeling of soil behavior with Hypoplasticity: Another Approach to soil constitutive modeling." Springer Series in Geomechanics and Geoengineering.

[24] .Mehdipour, I., Ghazavi, M., and Moayed, R.Z., (2013). "Numerical study on stability analysis of geocell reinforced slopes by considering the bending effect." Geotext. and Geomembr., 37, 23-34.

[25] Mehdipour, I., Ghazavi, M., and Moayed, R.Z., (2017). "Stability analysis of geocell reinforced slopes using the limit equilibrium horizontal slice method." Int. J. Geomech., 06017007, 1-15.

[26] Mohammadi-Haji B., and Ardakani A. (2018). "Numerical prediction of circular tunnel seismic behavior using hypoplastic soil constitutive model." Int J Geotech Eng. 1-14.

[27] Mohammadi-Haji B., and Ardakani A. (2020). "Performance based analysis of tunnel under seismic events with nonlinear features of soil mass and lining." Soil Dynamics and Earthquake Engineering, 134, 1-15.

[28] Song, F., Liu, H., Hu, H., and Xie, Y., (2018). "Centrifuge tests on geocell reinforced retaining walls at limit equilibrium." J. Geotech. Geoenvriron. Eng. 144(3): 04018005, 1-13.

[29] Song F., Tian Y. H. (2019). "Three-dimensional numerical modelling of geocell reinforced soils and its practical application." Geomechanics and Engineering, 17(1):1-9.

[30] Von Wolffersdorff, P.A. (1996). "A hypoplastic relation for granular materials with a predefined limit state surface." Mech. Cohesive Frict. Mater, 12, 51-71.

[31] Wu, W., and Kolymbas, D. (1990). " Numerical testing of the stability criterion for hypoplastic constitutive equations." Mechanics of Materials, 9(3), 245-253.

[32] Wu, W., and Bauer, E. (1994). "A simple hypoplastic constitutive model for sand." International Journal for Numerical and Analytical Methods in Geomechanics, 18(12), 833-862.

[33] Wu, W., and Kolymbas, D. (2000). "Hypoplasticity then and now." Constitutive modelling of granular materials, 57-105.

[34] Zhao, M.H., Zhang, L., Zou, X.J. and Zhao, H., (2009). "Research progress in two-direction composite foundation formed by geocell reinforced mattress and gravel piles." Chinese Journal of Highway and Transport 22(1), 1-10.